One-neutron knockout reaction of ^{17}C on a hydrogen target at 70 MeV/nucleon ☆

Y. Satou [a,*], J.W. Hwang [a], S. Kim [a], K. Tshoo [a], S. Choi [a], T. Nakamura [b], Y. Kondo [b], N. Matsui [b], Y. Hashimoto [b], T. Nakabayashi [b], T. Okumura [b], M. Shinohara [b], N. Fukuda [c], T. Sugimoto [c], H. Otsu [c], Y. Togano [c], T. Motobayashi [c], H. Sakurai [c], Y. Yanagisawa [c], N. Aoi [c], S. Takeuchi [c], T. Gomi [c], M. Ishihara [c], S. Kawai [d], H.J. Ong [e], T.K. Onishi [e], S. Shimoura [f], M. Tamaki [f], T. Kobayashi [g], Y. Matsuda [g], N. Endo [g], M. Kitayama [g]

[a] *Department of Physics and Astronomy, Seoul National University, 599 Gwanak, Seoul 151-742, Republic of Korea*
[b] *Department of Physics, Tokyo Institute of Technology, 2-12-1 Oh-Okayama, Meguro, Tokyo 152-8551, Japan*
[c] *RIKEN Nishina Center, 2-1 Hirosawa, Wako, Saitama 351-0198, Japan*
[d] *Department of Physics, Rikkyo University, 3 Nishi-Ikebukuro, Toshima, Tokyo 171-8501, Japan*
[e] *Department of Physics, University of Tokyo, 7-3-1 Hongo, Bunkyo, Tokyo 113-0033, Japan*
[f] *Center for Nuclear Study (CNS), University of Tokyo, 2-1 Hirosawa, Wako, Saitama 351-0198, Japan*
[g] *Department of Physics, Tohoku University, Aoba, Sendai, Miyagi 980-8578, Japan*

ARTICLE INFO

ABSTRACT

First experimental evidence of the population of the first 2^- state in ^{16}C above the neutron threshold is obtained by neutron knockout from ^{17}C on a hydrogen target. The invariant mass method combined with in-beam γ-ray detection is used to locate the state at 5.45(1) MeV. Comparison of its populating cross section and parallel momentum distribution with a Glauber model calculation utilizing the shell-model spectroscopic factor confirms the core-neutron removal nature of this state. Additionally, a previously known unbound state at 6.11 MeV and a new state at 6.28(2) MeV are observed. The position of the first 2^- state, which belongs to a member of the lowest-lying p–sd cross shell transition, is reasonably well described by the shell-model calculation using the WBT interaction.

© 2013 The Authors. Published by Elsevier B.V. All rights reserved.

Much of our knowledge on quantum nature of atomic nuclei comes from studies of nuclear reactions in which an energetic beam of one nuclear species collides with a target made of another. Among various collision processes, the nucleon knockout reaction has become recognized as one of the most sensitive tools for spectroscopic studies, especially for nuclei away from the stability line, which include even those beyond the drip line. The knockout residue produced by removing a nucleon (or nucleons) from a fast moving beam particle, which impinges on a light target fixed in the laboratory, is observed in inverse kinematics by a detector placed in forward hemisphere efficiently. The removed nucleon(s) will be selected democratically from the valence space, allowing states with unique, often rarely accessible configurations

to be populated in this process. The final state in the residue is identified by tagging de-excitation γ rays [1–3] (see also references in Ref. [4]) and by observing decay neutrons and constructing the invariant mass [5–12]. For one-nucleon knockout case, the momentum spread of the residue reflects the Fermi motion of the nucleon suddenly removed, and is sensitive to the orbital angular momentum (the l value) of the struck nucleon. Furthermore, the cross sections leading to individual final states relate to the occupancy of single-particle orbits, providing a link to details of the nuclear structure.

The present study aims at exploring unbound states in ^{16}C through an application of the one-neutron knockout technique to a ^{17}C beam impinged on a proton target, for which simple reaction mechanisms are expected. Focus is placed in a search of lowest-lying cross shell transitions, the location of which reflects the shell gap between p and sd orbits. The neutron-rich carbon (C) isotopes have attracted attention as they often exhibit unique features: none of the odd mass C (heavier than ^{13}C) has the ground-state spin parity of $J^{\pi}_{\text{g.s.}} = 5/2^+$, the values which are expected from a naive shell model. There has been a debate about a reduced E2 transition strength (small proton collectivity)

for the 2_1^+ state in ^{16}C [13–18]. There is evidence for neutron halo formation for ^{15}C [19], ^{19}C [20], and ^{22}C [21,22]. For some, if not all, of these features, nuclear deformation may play a key role, which occurs in this mass region due to near degeneracy of the $\nu d_{5/2}$–$\nu s_{1/2}$ orbits: neutrons in these orbits can gain energy by breaking spherical symmetry (the Jahn–Teller effect) [23]. The effect of nuclear deformation will further be signified by large quadrupole transition strengths [24,25] and by a reduction of the major p–sd shell gap [26–28]. A recent β-delayed neutron emission study of ^{17}B [29] has reported low-lying negative parity states in ^{17}C, among which the lowest one was the $J^\pi = 1/2^-$ state at the excitation energy of $E_x = 2.71(2)$ MeV. The energy of this state, reflecting the p–sd shell gap, turned out to be lower than those of neighboring odd mass C isotopes: $E_x = 3.10$ MeV for the $1/2_1^-$ state in ^{15}C and $E_x = 3.09$ MeV for the $1/2_1^+$ state in ^{13}C [30]. This might indicate an onset of the p–sd shell gap quenching towards heavier C isotopes. To examine this picture in more detail it is worthwhile to accumulate data on cross shell transitions in neighboring isotopes. This Letter reports on new relevant spectroscopic information on ^{16}C in its unbound E_x region. Besides, based on the parallel momentum distribution of the core fragment populated in a final state, it is demonstrated that the width of the distribution provides a good measure of the l value (and thus the parity) of the state populated; for neutron knockout involving a proton target, this has previously been shown based on the transverse momentum distributions in the ^{1}H(^{18}C, ^{17}C*) [31] and ^{1}H(^{14}Be, ^{13}Be*) [8] reactions with the aid of elaborate reaction mechanism calculations.

Despite relative proximity to stability, information on energy levels of ^{16}C, particularly that above the neutron threshold (the neutron separation energy of ^{16}C is $S_n = 4.250(4)$ MeV [32]), has been limited. This is partially due to ineffectiveness of β decay for this particular nucleus, as recognized by the absence of a parent nucleus (^{16}B is particle unstable). Early spectroscopic studies on ^{16}C utilized binary reactions involving transfers of neutrons. The ^{14}C(t, p)^{16}C two-neutron transfer studies [33–36] have investigated levels below 7 MeV, including six bound states and an unbound state at 6.11 MeV. Since the ground state of ^{14}C is characterized by neutron p-shell closure, the states populated mostly involved configurations with two sd-shell neutrons, $(1s0d)^2$. The ^{13}C(^{12}C, ^{9}C)^{16}C three-neutron transfer study [37] has reported 14 more states up to $E_x = 17.4$ MeV, including states with more complex configurations. Due to kinematical matching [37] states with high angular momenta were favorably populated. Combining information from the recent ^{15}C(d, p)^{16}C reaction study using a radioactive ^{15}C beam [17], sound J^π assignments have been available for bound states. For unbound states only the 8.92-MeV level has received a firm assignment of 5^- [37]. Two earlier one-neutron knockout studies on ^{17}C using Be targets focused on transitions leading to bound final states in ^{16}C by means of in-beam γ-ray spectroscopy [3,38]. They provided information not only on excited states of ^{16}C but also on ground state properties of ^{17}C, e.g., the spin parity, $J_{g.s.}^\pi(^{17}$C$) = 3/2^+$, and no halo formation in spite of the remarkable low neutron separation energy of $S_n = 0.727(18)$ MeV [32] due to a high angular momentum of $l = 2$ for the valence neutron.

The experiment was performed at the RIPS facility [39] of RIKEN. Details of the setup are provided in Refs. [25,40], and a preliminary report of this work has been presented in Ref. [41]. The ^{17}C beam was produced from a 110-MeV/nucleon ^{22}Ne beam which impinged on a 6-mm-thick Be target. The typical ^{17}C beam intensity was 10.2 kcps with a momentum spread of $\Delta P/P = \pm 0.1\%$. The beam profile was monitored by a set of parallel-plate avalanche counters (PPACs) placed upstream of the experimental target. The target was pure liquid hydrogen [42] contained in a
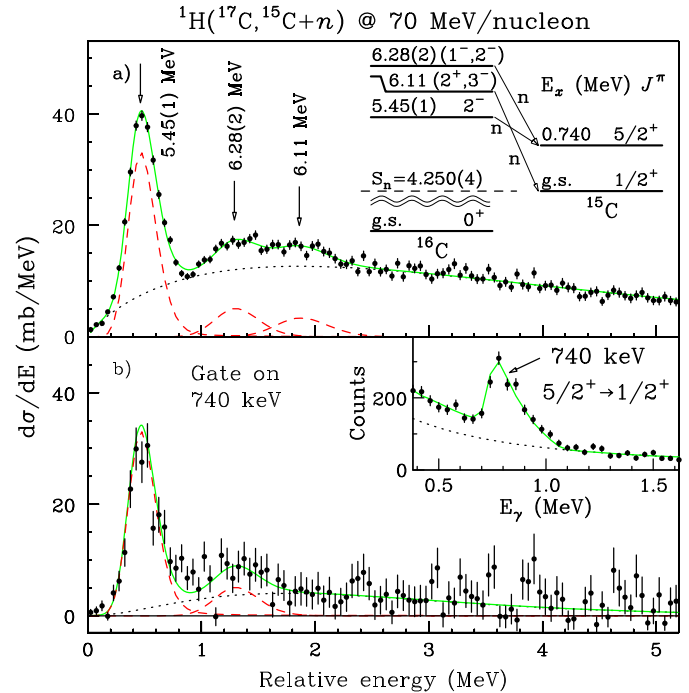

Fig. 1. (Color online.) Relative energy spectra for the (a) ^{1}H(^{17}C, ^{15}C + n) and (b) ^{1}H(^{17}C, ^{15}C($5/2^+$; 0.74 MeV) + n) one-neutron knockout reactions at 70 MeV/nucleon. Shown in the inset of panel (b) is the Doppler-corrected energy spectrum of γ rays emitted from ^{15}C. Neutron coincidence is required for this spectrum. Green solid lines represent the results of the fit; dotted lines assumed background; red dashed lines extracted individual resonances. A decay scheme for states populated is shown in panel (a).

cylindrical cell: 3 cm in diameter, 120 ± 2 mg/cm^2 in thickness, and having 6-μm-thick Havar foils for the entrance and exit windows. The average energy of ^{17}C at the middle of the target was 70 MeV/nucleon. The target was surrounded by a NaI(Tl) scintillator array used to detect γ rays from charged fragments. The fragment was bent by a dipole magnet behind the target, and was detected by a plastic counter hodoscope placed downstream of the magnet. The ΔE and time-of-flight (TOF) information in the hodoscope was used to identify the Z number of the fragment. The trajectory was reconstructed by a set of multi-wire drift chambers (MWDCs) before and after the magnet, which, together with TOF, gave mass identification. Neutrons were detected by two walls of plastic scintillator arrays placed 4.6 and 5.8 m downstream from the target. The neutron detection efficiency was $24.1 \pm 0.8\%$ for a threshold setting of 4 MeVee. The relative energy (E_{rel}) of the final system was calculated from momentum vectors of the charged fragment and the neutron. In deducing the fragment vector, information on the impact point on target in transverse directions (determined by the upstream tracking detectors) was taken into account together with hit information within the MWDC placed behind the target. Neutron coincidence events were classified in terms of E_{rel} and the Fermi momentum of the struck neutron k_3. In the sudden approximation, the latter corresponds to the transferred momentum to the knockout residue (^{16}C). The detector acceptance was evaluated by a Monte Carlo simulation as a function of E_{rel} and k_3.

Fig. 1 shows relative energy dependence of cross sections for the (a) ^{1}H(^{17}C, ^{15}C + n) and (b) ^{1}H(^{17}C, ^{15}C($5/2^+$; 0.74 MeV) + n) reactions at 70 MeV/nucleon. Background contributions measured by an empty target were subtracted. Error bars are statistical ones. Shown in the inset of Fig. 1(b) is the "Doppler-corrected" energy spectrum for γ rays emitted from the decay product nucleus ^{15}C. A peak around $E_\gamma = 0.8$ MeV arises from the decay of the

Table 1

States populated by the ^{1}H(^{17}C, ^{16}C) reaction. Theoretical cross sections were obtained by using the Glauber-model code csc_GM [45] and the shell-model spectroscopic factors calculated with the WBT interaction [46]. Calculations used S_n^{eff} involving experimental E_x values.

Experiment					Theory				J^π
E_{rel} (MeV)	E_x (MeV)	Γ (MeV)	l ($\hbar$)	σ_{-1n}^{exp} (mb)	E_x (MeV)	σ_{str} (mb)	σ_{diff} (mb)	σ_{-1n}^{th} (mb)	
0.463(3)[a]	5.45(1)	0.03(1)	1	10.6(6)	5.57	1.38	14.23	15.61	2_1^-
1.86[b]	6.11	–	–	$2.0^{+0.4}_{-0.8}$	5.75	0.05	0.53	0.58	(3_1^-)
					7.60	0.09	1.37	1.46	(2_3^+)
					8.81	0.04	0.31	0.35	(4_2^+)
1.29(2)[a]	6.28(2)	–	–	$2.5^{+0.2}_{-1.9}$	6.55	0.61	5.43	6.04	(1_2^-)
					6.63	0.28	2.57	2.85	(2_2^-)

[a] Observed in coincidence with the 0.74-MeV γ ray from ^{15}C.

[b] Derived from the energy $E_x = 6.11$ MeV in Ref. [33] by assuming the ^{15}C core is in the ground state.

first $5/2^+$ level at 0.74 MeV (the only bound excited state) to ^{15}C$_{g.s.}$. The $5/2^+$ state is an isomeric state having a half-life of 2.61 ± 0.07 ns [30]. This long life time caused the emission point of the de-excitation γ ray to be distributed along the path of the fast-moving decay product. The Doppler correction for the γ ray energy was made by assuming that the decay occurs at 40.7 cm downstream of the target (an average decay point expected from the average beam energy and the known mean life for the isomeric state) in both data reduction and simulation by the GEANT code [43]. The latter was done fully taking into account realistic geometry of the experiment. A higher energy tail for the photoelectric peak is due to this incomplete Doppler correction procedure. The simulated response, however, reproduced the data well as shown by the green solid line. The photo-peak efficiency over $E_\gamma = 0.60$–1.12 MeV (γ-ray window) was estimated to be 5.1(3)% by the GEANT simulation. Fig. 1(b) was obtained by gating on the $5/2^+$ γ peak with the above window and by correcting for the detection efficiency. The background component was subtracted by assuming (i) that the background portion is the same as that in the γ-ray spectrum in the inset of Fig. 1(b): the portion of the area beneath the dotted line over the γ-ray window, which amounts to 46%, and (ii) that the background shape is characterized by the inclusive spectrum in Fig. 1(a). A peak is clearly seen at $E_{rel} = 0.46$ MeV in Fig. 1(a). This is also evident in Fig. 1(b), indicating that this peak feeds the $5/2^+$ state in ^{15}C after emitting a neutron. Besides, another resonance is visible at $E_{rel} \approx 1.3$ MeV in Fig. 1(b). These were observed for the first time.

The relative energy spectrum of Fig. 1(a) was used in a fitting analysis to extract the parameters for the resonances: E_{rel} and the populating cross section σ_{-1n}^{exp}. Their responses (dashed lines) were generated by a Monte Carlo simulation which takes into account the detector resolution, beam profile, Coulomb multiple scattering, and range difference inside the target. The relative energy resolution was estimated to scale as $\Delta E_{rel} = 0.17\sqrt{E_{rel}}$ MeV (in rms). For the $E_{rel} = 0.46$-MeV state, a finite line width Γ for an $l = 1$ neutron emission was considered by adopting a single Breit–Wigner function [44,25] (for other states, not as well isolated in the present data as this state, only the instrumental resolution was taken into account). In the analysis an excess strength was recognized at $E_{rel} \approx 1.9$ MeV. This may correspond to the nearest known state at $E_x = 6.11$ MeV [33,36] if the decay product nucleus ^{15}C is populated in the ground state (in Fig. 1(a) the response of this strength was created by assuming $E_{rel} = 1.86$ MeV: the difference between $E_x = 6.11$ MeV and S_n for ^{16}C). A similar fitting analysis using the γ-ray coincidence spectrum in Fig. 1(b), however, did not exclude the possibility that this component is absent from this spectrum. It is quoted that the upper limit on the fraction of ^{15}C fragments from the decay of the $E_{rel} = 1.86$-MeV resonance, that were in the 0.74-MeV state is 20% of the strength found in the spectrum in Fig. 1(a). The solid line in Fig. 1(a) shows

the result of the fit to the total inclusive spectrum. The background (dotted line) coming from transitions to the continuum and from detecting neutrons not associated with the decay of excited states in ^{16}C, e.g., neutrons emitted from excited ^{17}C nuclei that are created by inelastic scattering processes, was simulated by a function $a(E_{rel})^b \exp(-cE_{rel})$ with a, b, and c free parameters. The results of the fit are summarized in Table 1. E_x was calculated by $E_x = E_{rel} + S_n + E^*$, with E^* the excitation energy of ^{15}C. The errors include statistical ones and those due to the choice of the background shape (the latter, estimated by further assuming thermal emission of a neutron ($b = 1/2$) and neutron evaporation ($b = 1$) for the background shape, turned out to be a dominant source of the error: they were 80, 90, and 70% of the errors quoted in Table 1 for E_{rel}, Γ, and σ_{-1n}^{exp}, respectively, for the $E_{rel} = 0.46$-MeV state, while they were 90, 20, and 70% in the (upper bounds of) errors of σ_{-1n}^{exp} for the $E_{rel} = 1.86$-MeV state and of E_{rel} and σ_{-1n}^{exp} for the $E_{rel} = 1.29$-MeV state, respectively). For σ_{-1n}^{exp}, uncertainties originating from the target thickness and neutron detection efficiency are included. The same fit was repeated for the γ-ray coincidence spectrum of Fig. 1(b) using the responses for the $E_{rel} = 0.46$ and 1.29-MeV states, obtained from the fit to the inclusive spectrum in Fig. 1(a). To quantify the character of the latter state, as a state built on the ^{15}C*(0.74 MeV) excited core, the fit was repeated by changing the strength from the original one. By finding the fractional value at which the χ^2 of the fit alters from the minimum by one unit, a lower limit of 32% was deduced. The extraction of the l value of the knocked-out neutron from a differential quantity for the $E_{rel} = 0.46$-MeV state is explained later.

To allow discussion in terms of nuclear structure, reaction model calculations based on the Glauber approximation [47] were performed. The one-neutron removal cross section σ_{-1n}^{th} is expressed for a given final state with J^π as

$$\sigma_{-1n}^{th} = \sum_{nlj} \left(\frac{A}{A-1}\right)^N C^2 S(J^\pi, nlj)\sigma_{sp}(nlj, S_n^{eff}), \qquad (1)$$

where A is the projectile mass, N the major oscillator quantum number, $C^2 S$ the spectroscopic factor, and σ_{sp} the single-particle cross section. The quantum numbers of the removed neutron are denoted by nlj. S_n^{eff} is the effective separation energy given by the sum of S_n of the projectile and E_x of the residue. σ_{sp} was calculated by the code csc_GM [45] taking into account both stripping and diffractive processes (effective nature of the nucleon–nucleon (NN) profile function used resulted in small non-zero stripping cross sections) [47]. The elastic S matrix for the collision of the residue (core) with the proton target was calculated by folding the finite-range Gaussian NN profile function [48] with the point proton and neutron densities of the core obtained from the Hartree–Fock (HF) calculation using the SkX interaction [49]. The S matrix
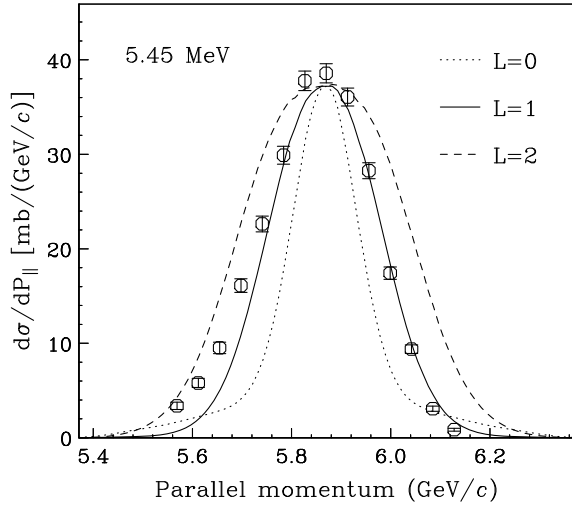
Fig. 2. Laboratory $p_\parallel$ distribution of ^{16}C populated in the 5.45-MeV state after knockout from ^{17}C (open circles). The dotted, solid, and dashed lines are the Fourier transform of single-particle wave functions of orbitals with $l = 0$, 1, and 2, respectively.
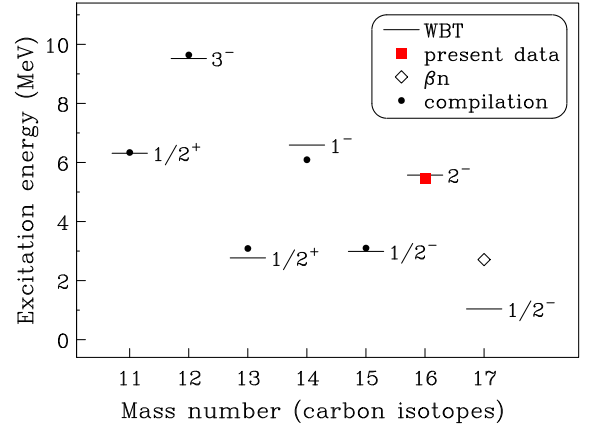

Fig. 3. (Color online.) The migration of energies of (known) lowest-lying states in C isotopes, whose parities are opposite to those of their respective ground states, in comparison to shell-model values obtained by using the WBT interaction [46]. Data for $^{11-15}$C (filled circles) are from Refs. [30,55]. The data point for ^{16}C (red filled square) is from the present study, while that for ^{17}C (open diamond) is from Ref. [29]. The shell-model calculations were performed within the 2$\hbar\omega$ and 0$\hbar\omega$ bases (for both positive and negative parity states) for $^{11-15}$C and ^{16,17}C, respectively.

for describing the scattering of the valence neutron with the target proton was given by $S(b) = 1 - \Gamma_{pn}(b)$, here b is the impact parameter of the colliding nucleons, and Γ_{pn} the profile function for proton–neutron scattering. The parameters chosen for the profile function are those describing the NN total and elastic cross sections consistently [48]. The neutron-residue relative motion was calculated in a Woods–Saxon potential. The depth was adjusted so as to reproduce S_n^{eff}, for a diffuseness $a_0 = 0.7$ fm and a reduced radius r_0 specifically chosen to be consistent with the HF calculation [50,51]: r_0 generates a single-particle wave function with a rms neutron-core separation of $r_{\text{sp}} = [A/(A-1)]^{1/2} r_{\text{HF}}$ at the HF-predicted binding energy, where r_{HF} is the HF rms radius of each orbit. The spin–orbit potential had the same a_0 and r_0 as the central one with a strength of -12 MeV in the notation of Ref. [52]. The HF radius for the $p_{1/2}$ ($p_{3/2}$) orbit of ^{17}C, for example, is 2.966 (2.779) fm; this translates into $r_{\text{sp}} = 3.057$ (2.865) fm, which is reproduced by taking $r_0 = 1.263$ (1.234) fm. The C^2S values were obtained by the shell-model code NUSHELL [53] using the WBT interaction [46] in the $spsdpf$ model space. The calculated results for relevant states are given in Table 1. σ_{-1n}^{th} includes contributions from both stripping (σ_{str}) and diffractive (σ_{diff}) mechanisms. Due to inert nature of the proton, the latter dominates the knockout processes.

The state observed at $E_x = 5.45$ MeV was found to be well explained by the 2_1^- shell-model state in both position and cross section, making an assignment of 2^- appropriate. The 2_1^- state exhibited the highest cross section of unidentified shell-model states in the energy region of interest. The summed σ_{-1n}^{th} for predicted 2^- and 1^- states below 8 MeV, where major strengths are concentrated, are 20.9 (15.5, 2.8, and 2.6 mb at $E_x = 5.57$, 6.63, and 7.23 MeV, respectively) and 11.5 mb (see below for composition), respectively. Their ratio is near to the statistical ratio of 5:3 expected for a doublet with spins $J = 2$ and 1, allowing an interpretation that the 2^- and 1^- states are formed by coupling a hole in the $\nu p_{1/2}$ orbit to three neutrons with $J = 3/2$ in the sd orbits (note that $J_{\text{g.s.}}^\pi$ (^{17}C) = $3/2^+$). The predicted 1^- strength is distributed among states at $E_x = 5.79$, 6.55, and 6.98 MeV with $\sigma_{-1n}^{\text{th}} = 0.6$, 6.0, and 4.9 mb, respectively. The fragmentation of the strength and the general trend in the Glauber model to overestimate the cross section [4,51] would exclude an assignment of 1^- for the 5.45-MeV state with $\sigma_{-1n}^{\text{exp}} = 10.6(6)$ mb.

Fig. 2 shows the laboratory parallel momentum ($p_\parallel$) distribution leading to the 5.45-MeV state. This was obtained by subdividing, in terms of $p_\parallel$, the inclusive spectrum and repeating the fitting procedure described above. The errors are statistical ones. Also plotted in Fig. 2 are the $p_\parallel$ distributions calculated with CSC_GM for varying l values. An experimental resolution of 43(1) MeV/c in rms is convoluted. Factors relevant to stripping mechanisms are dropped, and the curves represent the Fourier transform of the single-particle wave functions. The full width at half maximum (FWHM) of the experimental distribution for the 5.45-MeV state was determined by a fit using a Gaussian to be 210(11) MeV/c after unfolding the resolution. In the fit, a low-energy tail ($p_\parallel < 5.72$ GeV/c), which often suffers from higher-order effects [54], was eliminated. The fit curve (not shown) is similar to the $l = 1$ curve (solid line). The width agrees well with 233 MeV/c FWHM calculated for p-wave knockout, whereas for s- (dotted line) and d-wave (dashed line) knockout, widths of 121 and 377 MeV/c FWHM were respectively predicted, incompatible with the measurement. This observation agrees to the expected character of the 5.45-MeV, 2^- state as having a neutron hole in the p orbit, illustrating the robust feature of the $p_\parallel$ distribution as an l identifier.

The large populating cross sections observed for the 6.11-MeV state in the ^{14}C(t, p)^{16}C reactions [33,36] have suggested that this state is either of the natural parity 2^+, 3^-, or 4^+ states. The knockout cross sections calculated for the relevant 2_3^+, 3_1^-, and 4_2^+ shell-model states, together with their shell-model energies, are compared to the data in Table 1. The present data turned out not to provide a strong constraint on the J^π values for this state, although in terms of comparisons in both E_x and σ_{-1n} they seem to prefer the assignment of 2^+ or 3^-. The 6.28-MeV state exhibited the same decay pattern as the strongest 5.45-MeV 2^- state with a sizable cross section. The 1_2^- and 2_2^- states predicted at 6.55 and 6.63 MeV, respectively, had large populating cross sections and are candidates for this state.

The presently observed 2^-, 5.45-MeV state in ^{16}C belongs to a member of the lowest-lying states having an opposite parity to the ground state. The location of such states provides a measure of the p–sd shell gap and it is well explained by the shell model using the WBT interaction across the C isotopes, $^{11-15}$C. To illustrate the latter, their energies are compared to the shell-model values in

Fig. 3. In a recent study of β-delayed neutron emission of ^{17}B [29], three low-lying negative parity states were newly identified in just one-neutron heavier nucleus ^{17}C. The WBT interaction turned out to fail in predicting their location by about 1 MeV (theory predicts lower values, see also Fig. 3), and several possible mechanisms, such as reduction in pairing energy for neutrons in the sd orbits, were discussed. The present study adds a case in which the shell model with the WBT interaction predicts the location of the lowest-lying cross shell transition properly (see also Fig. 3), showing that this interaction describes the p–sd shell gap in ^{16}C adequately. To pin down the source of the discrepancy between theory and experiment on the position of the cross shell transition in ^{17}C, as discussed in Ref. [29], and to better understand the dynamical evolution of single-particle orbits and relevant residual interactions away from stability, further spectroscopic studies on such states in heavier C as well as neighboring isotopes are of help.

In summary, one-neutron knockout from ^{17}C on a proton target was exploited in populating two new states at 5.45(1) and 6.28(2) MeV, and a previously known state at 6.11 MeV in ^{16}C. The energy spectrum was constructed utilizing the invariant mass method involving a decay neutron and a ^{15}C fragment. De-excitation γ rays from the latter were measured to correctly locate the resonances. For the 5.45-MeV state, an attempt was made to deduce the orbital angular momentum of the knocked-out neutron from the parallel momentum distribution associated with the unbound knockout residue. This, together with a comparison in terms of the measured and calculated knockout cross sections, has led to a spin-parity assignment of 2^- for this state. Possible spins and parities have been suggested for the other states, bringing about an advanced understanding of the level scheme of ^{16}C. The energy of the first 2^- state was adequately reproduced by the standard shell-model calculation using the WBT interaction without invoking modifications to the residual interaction.

Acknowledgements

References

[1] A. Navin, et al., Phys. Rev. Lett. 81 (1998) 5089.
[2] T. Aumann, et al., Phys. Rev. Lett. 84 (2000) 35.
[3] V. Maddalena, et al., Phys. Rev. C 63 (2001) 024613.
[4] A. Gade, T. Glasmacher, Prog. Part. Nucl. Phys. 60 (2008) 161.
[5] H. Simon, et al., Phys. Rev. Lett. 83 (1999) 496.
[6] C.R. Hoffman, et al., Phys. Rev. Lett. 100 (2008) 152502.
[7] C.R. Hoffman, et al., Phys. Lett. B 672 (2009) 17.
[8] Y. Kondo, et al., Phys. Lett. B 690 (2010) 245.
[9] Z.X. Cao, et al., Phys. Lett. B 707 (2012) 46.
[10] E. Lunderberg, et al., Phys. Rev. Lett. 108 (2012) 142503.
[11] Yu. Aksyutina, et al., Phys. Lett. B 718 (2013) 1309.
[12] Z. Kohley, et al., Phys. Rev. Lett. 110 (2013) 152501.
[13] N. Imai, et al., Phys. Rev. Lett. 92 (2004) 062501.
[14] Z. Elekes, et al., Phys. Lett. B 586 (2004) 34.
[15] H.J. Ong, et al., Phys. Rev. C 78 (2008) 014308.
[16] M. Wiedeking, et al., Phys. Rev. Lett. 100 (2008) 152501.
[17] A.H. Wuosmaa, et al., Phys. Rev. Lett. 105 (2010) 132501.
[18] M. Petri, et al., Phys. Rev. C 86 (2012) 044329.
[19] E. Sauvan, et al., Phys. Lett. B 491 (2000) 1.
[20] T. Nakamura, et al., Phys. Rev. Lett. 83 (1999) 1112.
[21] K. Tanaka, et al., Phys. Rev. Lett. 104 (2010) 062701.
[22] N. Kobayashi, et al., Phys. Rev. C 86 (2012) 054604.
[23] I. Hamamoto, Phys. Rev. C 76 (2007) 054319.
[24] Z. Elekes, et al., Phys. Lett. B 614 (2005) 174.
[25] Y. Satou, et al., Phys. Lett. B 660 (2008) 320.
[26] L. Talmi, L. Una, Phys. Rev. Lett. 4 (1960) 469.
[27] T. Suzuki, T. Otsuka, Phys. Rev. C 56 (1997) 847.
[28] M. Wiedeking, et al., Phys. Rev. Lett. 94 (2005) 132501.
[29] H. Ueno, et al., Phys. Rev. C 87 (2013) 034316.
[30] F. Ajzenberg-Selove, Nucl. Phys. A 523 (1991) 1.
[31] Y. Kondo, et al., Phys. Rev. C 79 (2009) 014602.
[32] G. Audi, A.H. Wapstra, C. Thibault, Nucl. Phys. A 729 (2003) 337.
[33] H.T. Fortune, et al., Phys. Lett. B 70 (1977) 408.
[34] D.P. Balamuth, et al., Nucl. Phys. A 290 (1977) 65.
[35] H.T. Fortune, et al., Phys. Rev. Lett. 40 (1978) 1236.
[36] R.R. Sercely, et al., Phys. Rev. C 17 (1978) 1919.
[37] H.G. Bohlen, et al., Phys. Rev. C 68 (2003) 054606.
[38] C. Rodriguez-Tajes, et al., Eur. Phys. J. A 48 (2012) 95.
[39] T. Kubo, et al., Nucl. Instrum. Methods Phys. Res. Sect. B 70 (1992) 309.
[40] K. Tshoo, et al., Phys. Rev. Lett. 109 (2012) 022501.
[41] J.W. Hwang, et al., Few-Body Syst. 54 (2013) 1469.
[42] H. Ryuto, et al., Nucl. Instrum. Methods Phys. Res. Sect. A 555 (2005) 1.
[43] GEANT, Cern Library Long Writeup W5013, 1994.
[44] A.M. Lane, R.G. Thomas, Rev. Mod. Phys. 30 (1958) 257.
[45] B. Abu-Ibrahim, et al., Comput. Phys. Commun. 151 (2003) 369.
[46] E.K. Warburton, B.A. Brown, Phys. Rev. C 46 (1992) 923.
[47] P.G. Hansen, J.A. Tostevin, Annu. Rev. Nucl. Part. Sci. 53 (2003) 219.
[48] B. Abu-Ibrahim, et al., Phys. Rev. C 77 (2008) 034607.
[49] B.A. Brown, Phys. Rev. C 58 (1998) 220.
[50] J.R. Terry, et al., Phys. Rev. C 69 (2004) 054306.
[51] A. Gade, et al., Phys. Rev. C 77 (2008) 044306.
[52] C.A. Bertulani, A. Gade, Comput. Phys. Commun. 175 (2006) 372.
[53] B.A. Brown, W.D.M. Rae, MSU-NSCL report, 2007.
[54] J.A. Tostevin, et al., Phys. Rev. C 66 (2002) 024607.
[55] F. Ajzenberg-Selove, Nucl. Phys. A 506 (1990) 1.